Int. J. Heat Mass Transfer. Vol. 34, No. 12, pp. 3083–3095, 1991
Printed in Great Britain

0017–9310/91 $3.00+0.00

Lumped-parameter modeling of heat transfer enhanced by sinusoidal motion of fluid

MAMORU OZAWA†
Department of Production Engineering, Kobe University, Rokkodai-cho 1-1, Nada, Kobe 657, Japan

and

AKIRA KAWAMOTO
Osaka Works, Toshiba Co., Ohta-toshiba-cho 1-6, Ibaraki 567, Japan

(*Received* 22 *October* 1990 *and in final form* 8 *January* 1991)

Abstract—By imposing a sinusoidal motion on the fluid in a pipe, axial heat transfer was highly enhanced. This was mainly owing to lateral diffusion of heat, accumulation capacity of heat in a region of depth of penetration formed near the wall and convective motion forced by the oscillation. Numerical simulation and thermal-flow visualization gave a phenomenological explanation of the fundamental heat transfer mechanism. The effective thermal diffusivity in the axial direction was formulated based on the lumped-parameter heat transfer model, and the constitutive relationship of the lateral heat transfer was derived from the simulation and experiments.

1. INTRODUCTION

INCREASING attention has been given to the development of technologies for heat transfer enhancement as well as heat transfer control. Recently, Kurzweg and his co-workers [1–4] have developed new technology for the enhancement of heat transfer by sinusoidal oscillation of a fluid, i.e. heat transfer in a pipe connected to hot and cold reservoirs at both ends has been highly enhanced by imposing sinusoidal oscillation. Their system has been referred to as the 'dream pipe'. In such oscillating flow, significant phase lag of velocity variation appears between the fluid in the bulk and that near the wall, and a boundary layer which is referred to as the depth of penetration is formed in the wall region [5]. Lateral heat transfer between the bulk and the depth of penetration and axial displacement by sinusoidal oscillation enhance the axial heat transfer through the pipe [1, 2].

By imposing an oscillatory motion on the fluid, heat transfer performance is kept at a high level, otherwise the heat transfer performance drops significantly to a very low level of heat conduction. Moreover, heat transfer depends significantly on the frequency and amplitude of the oscillation imposed. Regulating the frequency and amplitude, the heat transfer performance can be brought to a predetermined level. Thus, this heat transfer mechanism will be applicable to heat transfer control.

Kurzweg and Zhao [1] and Kurzweg [2] have conducted experimental and analytical investigations by using the dream pipe model with a rather complicated configuration. They proposed a simplified heat transfer mechanism as well as characteristic parameters which represented the heat transfer performance. However, the complicated configuration of the test section adversely affects the fundamental understanding of the phenomena as well as the generality of the results. Thus, their experimental results are hardly applicable to other systems with different geometrical configurations. Recently, Zhang and Kurzweg [4] have conducted numerical simulation of such a dream pipe, where the depth of penetration near the wall has been taken into account only as an accumulation capacity of heat, and the motion of fluid in the wall region has not been taken into account, i.e. the depth of penetration has a priori been given in the simulation. This would lead to misunderstanding of the time-dependent behavior of the temperature profile as well as the heat transfer mechanism. For a fundamental understanding of the heat transfer mechanism as well as better estimation of the heat transfer performance available in the design and planning of the system, it is necessary to carry out further experimental or numerical investigations using a simple geometrical configuration, such as a single pipe, and also to conduct simplified and phenomenological modeling.

Thus, in this paper, firstly numerical simulation of the dream pipe is conducted by using a two-dimensional flow model, and the validity of the simulation is examined through comparison with the experimental results of thermal-flow visualization of the dream pipe. Based on the mechanism suggested by the simu-

† Present address: Department of Mechanical Engineering, Kansai University, Yamate-cho 3-3-35, Suita 564, Japan.

NOMENCLATURE

B	half value of channel width
$\delta B, \delta r$	depth of penetration
C_p	specific heat
D	pipe diameter
f	frequency
$\mathbf{g}$	gravitational acceleration
L	channel length
δL	amplitude of oscillation of bulk fluid
ΔL	superficial amplitude of fluid
m	number of cells
Nu_{eff}	Nusselt number
P	pressure
Pr	Prandtl number
Q	lateral heat flux per unit depth
Q_a	axial heat transfer rate per unit depth
r	radius
Re_m	modified Reynolds number
t	time
T	temperature
T_b	temperature in the bulk
T_f	temperature in the region of depth of penetration
δT	amplitude of temperature oscillation
ΔT	temperature difference
$\mathbf{V}$	velocity
z	vertical coordinate.

Greek symbols

α_{eff}	effective heat transfer coefficient
ζ, ξ	normalized depth of penetration
κ	thermal diffusivity
κ_d	effective thermal diffusivity
κ_{eff}	effective thermal diffusivity enhanced by oscillation
λ	thermal conductivity
λ_{eff}	effective thermal conductivity
ν	kinematic viscosity
ρ	density
τ	viscous stress tensor
τ	characteristic time constant
τ_d	delay time
τ_d^*	normalized delay time.

Subscripts

b	bulk fluid
f	depth of penetration
i	value in the ith cell.

Superscript

(n)	value at the nth time step.

lation results, a simplified lumped-parameter heat transfer model is developed, and the transient behavior and characteristic parameters are formulated.

2. NUMERICAL SIMULATION

Numerical simulation was conducted using a two-dimensional flow model. The fundamental equations are listed below:

$$\partial\rho/\partial t + \text{div}(\rho\mathbf{V}) = 0 \tag{1}$$

$$\rho D\mathbf{V}/Dt = -\text{grad}\, P + \rho\mathbf{g} - \text{div}\,\tau \tag{2}$$

$$\rho C_p DT/Dt = \text{div}(-\lambda\,\text{grad}\, T) \tag{3}$$

where ρ represents the density of fluid, t the time, $\mathbf{V}$ the velocity vector, P the pressure, $\mathbf{g}$ the gravitational acceleration, τ the viscous stress tensor, C_p the specific heat, T the temperature and λ the thermal conductivity. Boundary conditions adopted in the present simulation were no-slip and adiabatic conditions at the side walls, and continuous flow condition at the upper boundary, while the velocity V_{in} at the lower boundary was given by

$$V_{in} = V_0 \sin(2\pi f t), \quad V_0 = \Delta L \pi f \tag{4}$$

where V_0 represents the mean volumetric flux per half-cycle and ΔL the total volume flowing into the channel during the half-cycle divided by the cross-sectional area and is referred to as the superficial amplitude in this paper. In the present calculation, the width of the channel was set to 9 mm which coincides with that in the thermal-flow visualization experiment described later, while the length of the channel was set to 10 mm. These equations were solved numerically under Boussinesq's approximation. The numerical scheme applied to the present problem was the same as the finite difference scheme for the mixed-convection of Tomiyama *et al.* [6] which was similar to that of the SMAC method.

Figures 1 and 2 show the velocity and temperature profiles during one cycle. Dashed curves represent the velocity profiles in the middle position along the channel and the solid lines the isotherms. The horizontal dot–dash line is the coordinate of the vertical velocity $V = 0$. The velocity profile is relatively flat in the bulk, while the velocity changes drastically near the wall. Referring to the case of $f = 0.04$ Hz, the history of the velocity profile during one cycle clearly indicates the existence of phase lag between the fluid motion in the bulk and that in the wall region. This is also true in the case of $f = 0.32$ Hz, while the phase lag in the latter case is much larger than the former case, and reaches almost 300 deg, i.e. the phase lag increases with the increase in the oscillation frequency. Vertical dot–dash lines indicate the positions of the depth of penetration calculated by equation (5) [5]

$$\delta B = \sqrt{(\nu/\pi f)}. \tag{5}$$

The position of the depth of penetration by equation

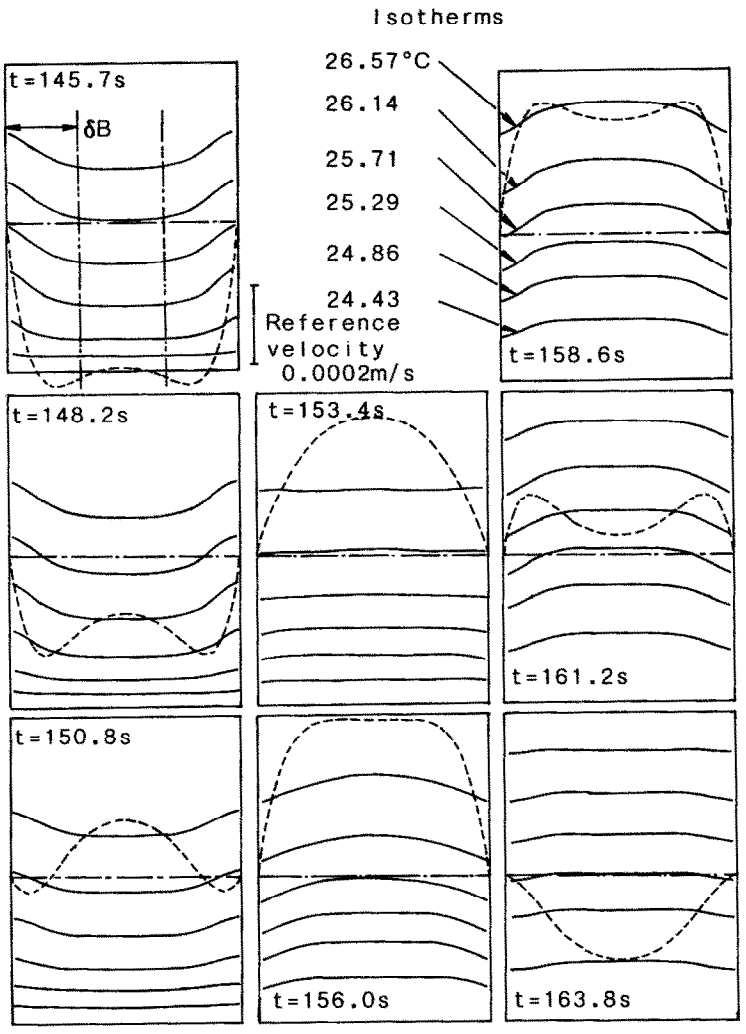

FIG. 1. Velocity and temperature profiles ($T_H = 26.9°C$, $T_L = 24.2°C$, $Pr = 7.90$, $f = 0.04$ Hz, $\Delta L = 3.0$ mm).

(5) approximately corresponds to the thickness of the velocity boundary layer.

Isotherms are drawn for every 0.43 K in each figure. Isotherms change significantly from the shape with an upward peak to that with a downward peak. The change in the isotherm's shape follows that of the velocity profile with a certain phase lag. Comparing the vertical dot–dash lines with the isotherms, it seems that the position of the dot–dash line approximately coincides with the thickness of the thermal boundary layer. This means that the thermal boundary layer, or the lateral temperature gradient is formed, in principle, owing to the velocity profile or the phase lag between the fluid motions in the region of the depth of penetration near the wall and in the bulk of the channel. Thus, the thickness of the thermal boundary layer coincides with that of the velocity boundary layer in such flow field with sinusoidal fluid oscillation. Zhang and Kurzweg [4] reported that the thickness of the thermal boundary layer is given by $\delta B/Pr$, which might be deduced from the analogy with a forced convective heat transfer. However, such a relationship does not hold in the present range of simulation, $Pr = 2$–100.

Referring to the isotherms in Fig. 1 for $f = 0.04$ Hz, the heat transfer mechanism can be explained phenomenologically. In the first figure, $t = 145.7$ s, the temperature in the bulk fluid is higher than that in the region of the depth of penetration. Thus, the heat transfer takes place in the direction from the bulk to the depth of penetration. In the next step, the fluid which is initially located at the lower position rises and the isotherm has an upward peak ($t = 148.2$–156.0 s). At this stage, the temperature in the region of the depth of penetration is higher than that in the bulk, and heat transfer is directed from the depth of penetration to the bulk ($t = 156.0$–161.2 s). The fluid in the bulk is warmed up and then transfered down-

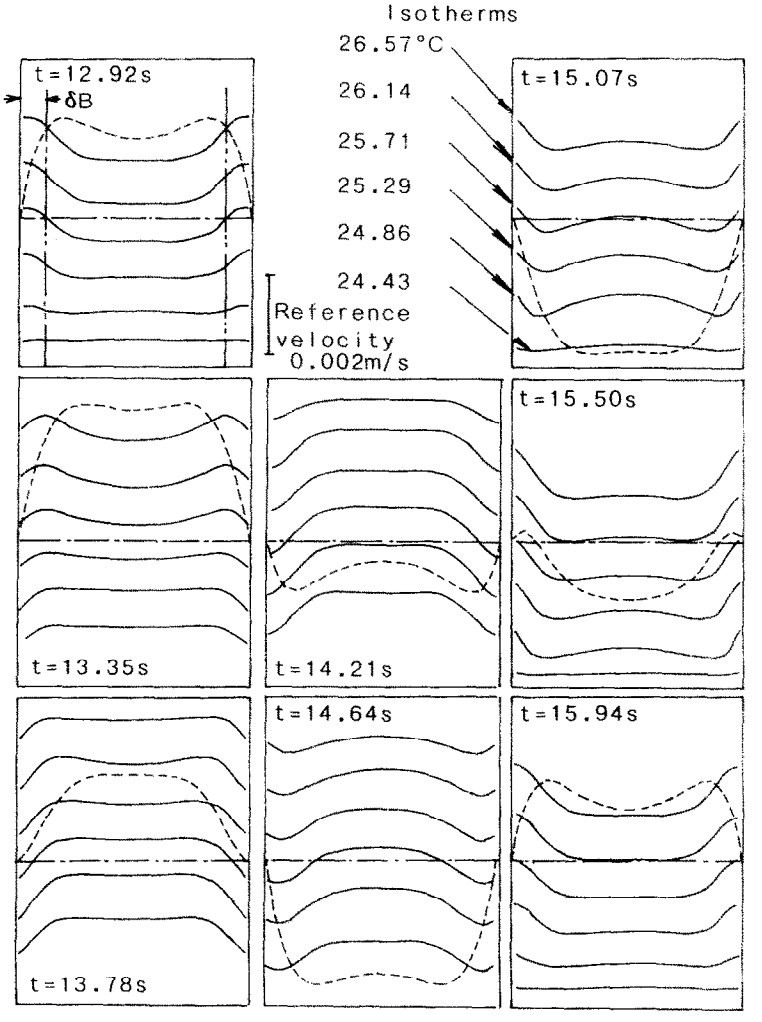

FIG. 2. Velocity and temperature profiles ($T_H = 26.9$ C, $T_L = 24.2$ C, $Pr = 7.90$, $f = 0.32$ Hz, $\Delta L = 3.0$ mm).

ward ($t = 161.2$–163.8 s). These processes repeat successively. Thus, heat transfer enhancement owing to such sinusoidal oscillation is dominated by three mechanisms; the lateral diffusion of heat owing to the temperature gradient caused by the phase lag of the fluid motion, an accumulation capacity of heat in the region of the depth of penetration, and the axial convection forced by the sinusoidal fluid motion in the bulk. The last mechanism is, in other words, considered to be some kind of pumping action for heat. Besides this heat transfer mechanism, axial heat conduction still exists. For example, the heat conduction dominates the axial heat transfer in the case of a liquid metal, such as mercury. In this case, the isotherms become flat owing to the high conductivity and, therefore, the effect of the lateral diffusion and hence the enhancement of heat transfer are relatively weak in the axial heat transfer performance.

3. THERMAL FLOW VISUALIZATION BY MEANS OF A THERMO-SENSITIVE LIQUID-CRYSTAL TRACER TECHNIQUE

The temperature profile in the dream pipe model with a rectangular cross-section was visualized by means of a thermo-sensitive liquid-crystal tracer technique. Figure 3 shows a schematic diagram of the experimental apparatus used. The working fluid was water. The test section was 9×9 mm in cross-section and 200 mm in length. The upper and lower ends of the test section were connected to the plenums. Heating and cooling pipes were inserted in both plenums to maintain constant temperature in the plenums during the experiment. Slits of 2 mm in width at the side walls permitted the light sheet to be formed in the test channel. The temperature profile was visualized by mixing liquid-crystal tracers of a chiral nematic type

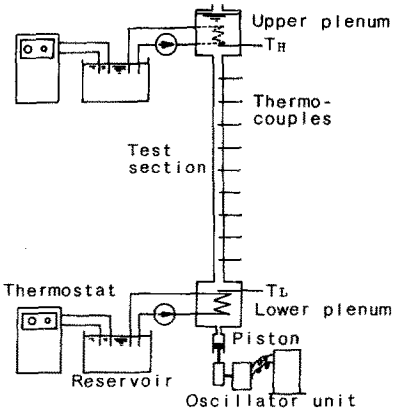

FIG. 3. Experimental apparatus.

(KW2535 of Japan Capsular Products Inc.). The density of the tracer particle was approximately equal to that of water and the particle diameter was about 15–20 μm. Thus, it was considered that the tracer particles were neutrally buoyant. Temperatures T_H and T_L in the upper and lower plenums were 26.9 and 24.2°C, respectively. The superficial amplitude $\Delta L = 44.8$ mm was imposed on the test fluid.

Figures 4 and 5 are photographs taken during one cycle. Each color corresponds to a certain temperature, thus the pictures represent the isotherms in the channel. The color changes through blue, green, yellow, red and brown down the test channel. This order of color indicates that the temperature decreases from the top of the test channel to the bottom.

With reference to the pictures for $f = 0.32$ Hz in Fig. 5, the phenomena observed in the test channel are explained in succession. At time $t = 0$, the bulk fluid in the center of the channel was moving upward, while the fluid in the wall region stayed still. When the bulk fluid stopped moving, the fluid in the wall region began to move downward ($t = 0.285$ s). During the period $t = 0.57$–1.140 s, most of the fluid moved downward in both regions. The bulk fluid continued to move downward at $t = 1.425$ s, while the fluid in the wall region stopped moving. When the bulk fluid stopped moving, the fluid in the wall region had already moved upward. Such phase lag in the movement between the bulk and the wall region is quite similar to that obtained in the numerical simulation shown in the previous section. Moreover, the shape of isotherms in Figs. 4 and 5 are quite similar to those in Figs. 1 and 2, respectively. Thus, the present pictures obtained in the thermal-flow visualization confirm the applicability of the present simulation to this heat transfer problem with sinusoidal oscillation.

4. TIME-DEPENDENT BEHAVIOR OF MEAN TEMPERATURE AND AXIAL HEAT TRANSFER

4.1. *Time-dependent behavior of mean temperature*

Unsteady heat transfer behavior was simulated by means of the present numerical scheme. The geometrical dimensions in this simulation were 3.4 mm in width and 15 mm in length. The width of the channel was equal to the diameter of one of the test pipes in the experiment described later. On the other hand, the length of the channel in the simulation is short compared with that in the experiment; that is mainly due to the limitation in the computation time. The temperature of the upper boundary was set at $T_H = 26.5$°C, that of the lower boundary at $T_L = 24.5$°C, and the initial temperature in the channel was set to be equal to T_L.

Figure 6 represents one of the examples of the temperature history obtained in the simulation. The data presented are those for $z/L = 4.5/30$, $14.5/30$, and $24.5/30$ along the channel axis. The smooth solid lines represent the mean temperature history. The temperature gradually increases with oscillation at a certain amplitude. This amplitude becomes larger with the increase in the height z/L. The amplitude decreases with time higher up the channel, while it increases with time lower down the channel. When the heat transfer process is fully developed, the amplitude of the temperature oscillation will become equal throughout the channel, and at the same time, the mean temperature during the oscillation will show a linear distribution along the channel.

In order to characterize the response speed of the temperature increase, we introduce here the delay time τ_d which is defined as the time when the mean temperature reaches the mean value T_M of the initial temperature T_L and the settling temperature T_S, i.e. $T_M = (T_S + T_L)/2$, where the settling temperature at the position z/L is given by

$$T_S = T_L + (T_H - T_L)z/L. \tag{6}$$

The delay time τ_d, in general, decreases exponentially with the increase in the oscillation frequency. When the amplitude of oscillation ΔL becomes large, the delay time τ_d decreases significantly.

It is necessary to obtain the axial heat flux for the estimation of the heat transfer performance in the present system. However, it was rather difficult to obtain the data of the axial heat flux in the experiments. Thus in the present stage of investigation, we introduced the effective thermal diffusivity as a representative performance which could be obtained both in the simulation and in the experiment.

In the following, the effective thermal diffusivity is derived based on an analogy between the present problem and the unsteady heat conduction problem. Under the condition of constant temperatures at both ends, T_H and T_L, and the initial temperature T_L at any position, the temperature history of one-dimensional heat conduction is given analytically by [7]

$$\frac{T - T_L}{T_H - T_L} = \frac{z}{L} + \frac{2}{\pi}\sum_{s=1}^{\infty}\frac{(-1)^s}{s}\exp\left(-\frac{\kappa s^2\pi^2}{L^2}t\right)\sin\left(\frac{s\pi z}{L}\right) \tag{7}$$

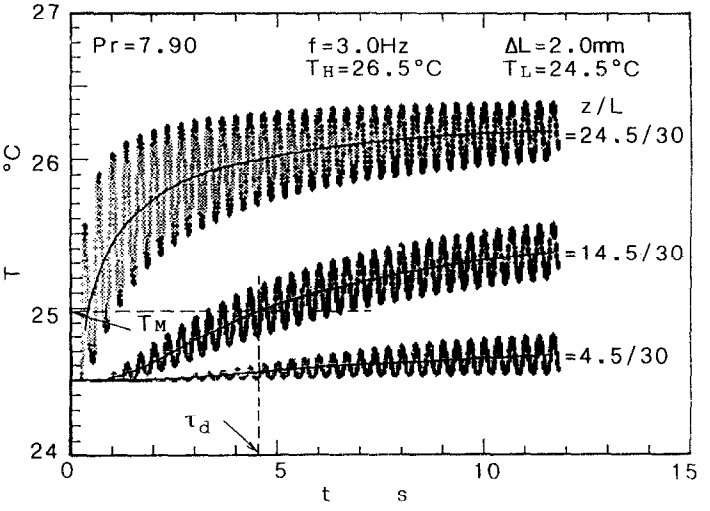

FIG. 6. Temperature response (numerical simulation).

where κ represents the thermal diffusivity of material. The normalized temperature $(T-T_L)/(T_H-T_L)$ is expressed as a function of the position z/L and the normalized time $\kappa t/L^2$.

Providing that the mean temperature history in the present problem is analogous to that of the unsteady heat conduction in the normalized form, we can define the effective thermal diffusivity. Using equation (7), the normalized delay time τ_d^* in the heat conduction is defined in the same manner as described above, i.e. the value $\kappa t/L^2$ corresponding to the normalized temperature $(T_M-T_L)/(T_H-T_L)$ on the temperature history curve. At the position $z/L = 14.5/30$, the normalized delay time τ_d^* becomes $\tau_d^*(\equiv \kappa_d\tau_d/L^2) = 0.098$. Then the effective thermal diffusivity κ_d is given by

$$\kappa_d = \tau_d^* L^2/\tau_d. \tag{8}$$

Substituting τ_d obtained in the numerical simulation into equation (8), the effective thermal diffusivity κ_d is calculated.

The axial heat transfer is mainly determined by two factors: the axial heat conduction and the enhanced heat transfer by oscillation. The heat transfer performance is a combination of these two factors. When the thermal conductivity of the fluid is very large, the heat conduction dominates the axial heat transfer. On the other hand, when the thermal conductivity is small enough the enhanced heat transfer by oscillation dominates the axial heat transfer. When the working fluid is mercury, as a typical example, the thermal diffusivity is $\kappa = 4.57\times10^{-6}\ m^2\ s^{-1}$ and the effective thermal diffusivity becomes $\kappa_d = 6.37\times10^{-6}\ m^2\ s^{-1}$ in the simulation for $f = 1.0$ Hz and $\Delta L = 2.0$ mm. On the other hand, such values are $\kappa = 1.41\times10^{-7}\ m^2\ s^{-1}$ and $\kappa_d = 1.48\times10^{-6}\ m^2\ s^{-1}$ for water, respectively. Hence, the contribution of the thermal diffusivity κ should be subtracted from the effective thermal diffusivity κ_d in order to discuss the enhancement of heat transfer. Then, in this report the effective thermal diffusivity κ_{eff} enhanced by oscillation is given by

$$\kappa_{eff} = \kappa_d - \kappa. \tag{9}$$

In the next section, the one-dimensional lumped-parameter heat transfer model is developed and the effective thermal diffusivity enhanced by oscillation is formulated analytically.

4.2. *Lumped-parameter heat transfer model*

The important mechanisms in the present phenomena are the lateral diffusion of heat, the accumulation capacity of heat, and the forced convective motion in the bulk. The simplified lumped-parameter model is constructed so as to realize such mechanisms as shown in Fig. 7. The flow field is divided into two parts, i.e. the region of the depth of penetration δB near the wall and the bulk region in the center. The fluid in the region of the depth of penetration stays still and the sinusoidal motion of the bulk fluid is

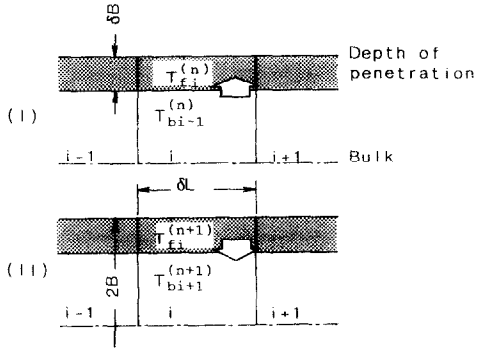

FIG. 7. Lumped-parameter heat transfer model.

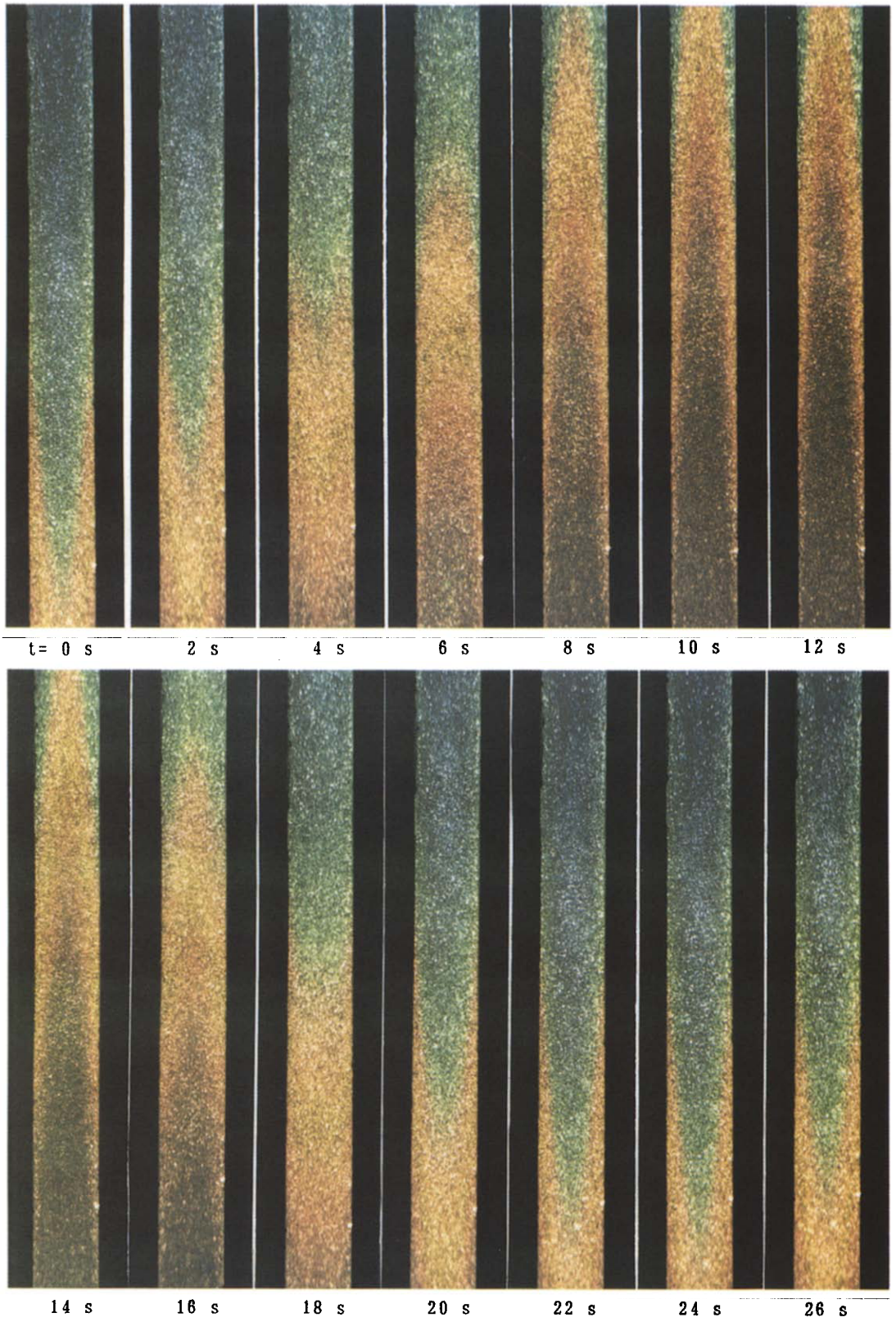

FIG. 4. Visualized image by using liquid-crystal tracer ($T_H = 26.9°C$, $T_L = 24.2°C$, $Pr = 7.90$, $f = 0.04$ Hz, $\Delta L = 44.8$ mm).

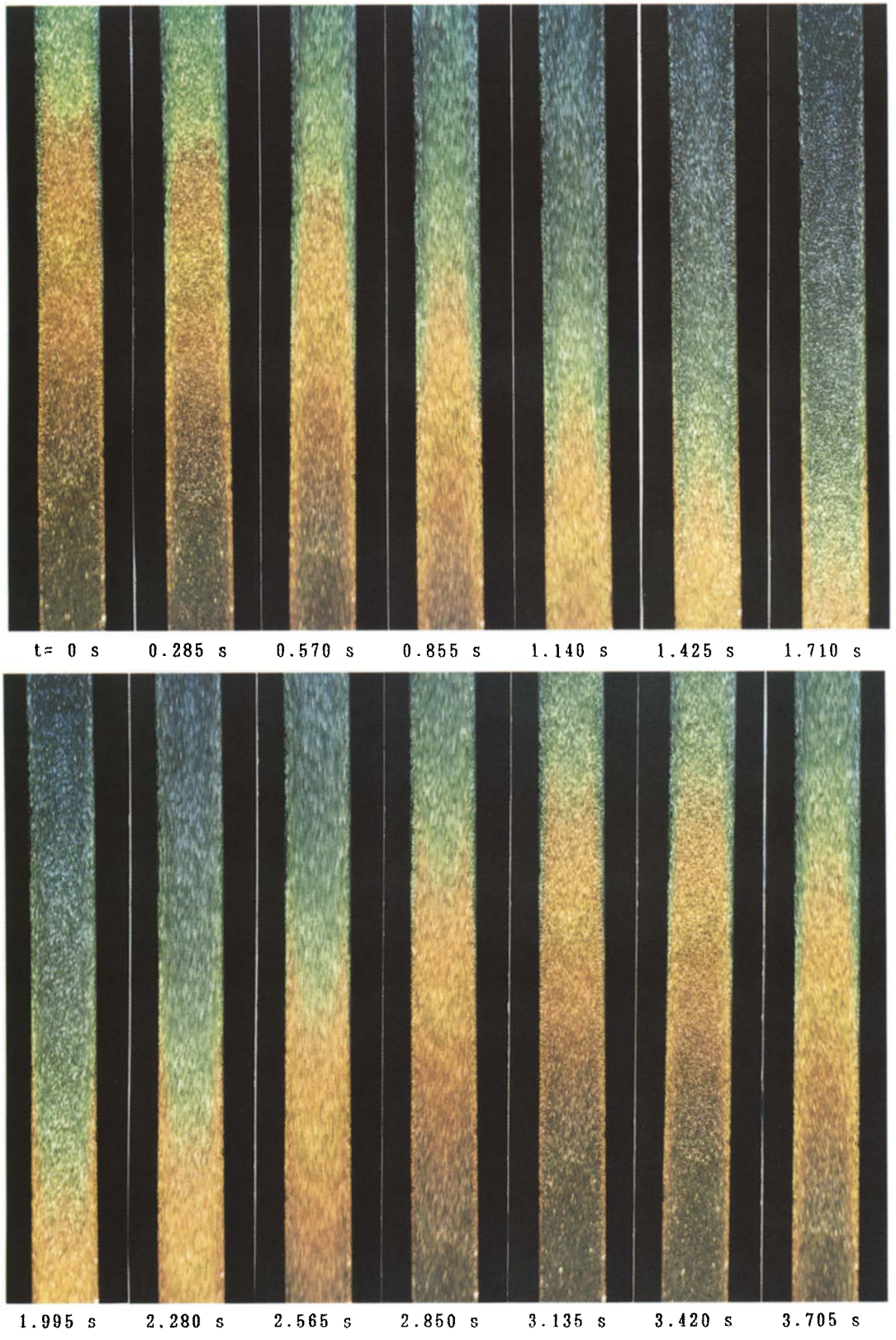

FIG. 5. Visualized image by using liquid-crystal tracer ($T_H = 26.9$°C, $T_L = 24.2$°C, $Pr = 7.90$, $f = 0.32$ Hz, $\Delta L = 44.8$ mm).

approximated by the square wave of period $2\delta t(=1/f)$ and the amplitude δL. At the time $(n)\times\delta t$, the higher temperature fluid of $T_{bi+1}^{(n)}$ in the upstream $(i-1)$th cell flows into the ith cell, and heat transfer takes place in the direction from the bulk to the depth of penetration (Process I). After a half-period δt, the lower temperature fluid of $T_{bi+1}^{(n+1)}$ in the $(i+1)$th cell flows into the ith cell. Then the heat transfer takes place in the direction from the depth of penetration to the bulk (Process II).

The lateral heat transfer between the two regions and the temperature variation in both regions are expressed by

$$Q_i = 2\delta L\alpha_{\text{eff}}(T_{bi}-T_{fi}) \tag{10}$$

$$Q_i = -2(B-\delta B)\delta L\rho C_p\frac{dT_{bi}}{dt} \tag{11}$$

$$Q_i = 2\delta L\delta B\rho C_p\frac{dT_{fi}}{dt} \tag{12}$$

where B represents a half-value of the channel width, Q_i the lateral heat flux per unit depth in the ith cell, α_{eff} the effective heat transfer coefficient between the bulk and the region of the depth of penetration. Considering the existence of the depth of penetration, amplitude δL is given by

$$\delta L = \Delta LB/(B-\delta B). \tag{13}$$

Eliminating Q_i and T_{fi}, we obtain the differential equation for T_{bi}

$$\frac{d}{dt}\left(\frac{dT_{bi}}{dt}+\frac{1}{\tau}T_{bi}\right)=0 \tag{14}$$

where τ represents the characteristic time constant relating to the lateral heat transfer and the heat capacity, and is given by

$$\tau = \frac{\rho C_pB}{\alpha_{\text{eff}}}\zeta(1-\zeta) \tag{15}$$

and ζ represents the normalized depth of penetration

$$\zeta = \delta B/B(\equiv\sqrt{(v/\pi f)}/B). \tag{16}$$

Solving equation (14) under the conditions $T_{bi}=T_{bi-1}^{(n)}$ and $T_{fi}=T_{fi}^{(n)}$ at $t=0$, and $T_{bi}=T_{fi}$ at $t=\infty$ for Process I, the temperature response in the bulk and that in the region of the depth of penetration are given by

$$T_{bi}^{(n+1)}-T_{bi-1}^{(n)} = -\zeta[1-\exp(-\delta t/\tau)](T_{bi-1}^{(n)}-T_{fi}^{(n)}) \tag{17}$$

$$T_{fi}^{(n+1)}-T_{fi}^{(n)} = (1-\zeta)[1-\exp(-\delta t/\tau)](T_{bi-1}^{(n)}-T_{fi}^{(n)}). \tag{18}$$

In the same manner, the temperature response for Process II is obtained under the conditions $T_{bi}=T_{bi+1}^{(n+1)}$ and $T_{fi}=T_{fi}^{(n+1)}$ at $t=0$, and $T_{bi}=T_{fi}$ at $t=\infty$

$$T_{bi}^{(n+2)}-T_{bi+1}^{(n+1)} = -\zeta[1-\exp(-\delta t/\tau)](T_{bi+1}^{(n+1)}-T_{fi}^{(n+1)}) \tag{19}$$

$$T_{fi}^{(n+2)}-T_{fi}^{(n+1)} = (1-\zeta)[1-\exp(-\delta t/\tau)](T_{bi+1}^{(n+1)}-T_{fi}^{(n+1)}). \tag{20}$$

Calculation of equations (17)–(20) gives the temperature response at every successive time step and cell.

4.3. *Effective thermal diffusivity*

When the axial heat transfer is fully developed, the amplitude at every position as well as the temperature difference between each successive two cells are uniform along the channel. Then, we define the amplitude δT_i and temperature difference ΔT_i by

$$\delta T_i \equiv T_{bi}^{(n+2)}-T_{bi+1}^{(n+1)} = -(T_{bi}^{(n+1)}-T_{bi-1}^{(n)}) \tag{21}$$

$$\Delta T_i \equiv T_{bi-1}^{(n)}-T_{bi}^{(n)}. \tag{22}$$

Furthermore, the next relationship holds under the fully developed condition

$$T_{bi}^{(n)} = T_{bi}^{(n+2)}. \tag{23}$$

Substituting equations (21)–(23) into equations (17)–(20), and eliminating T_{fi} from equations (17) to (20), we have

$$\delta T = \frac{1}{m}\zeta\frac{1-\exp(-1/2f\tau)}{1+\exp(-1/2f\tau)}\Delta T \tag{24}$$

where $\delta T_i=\delta T$ and

$$\Delta T = \sum_m(\Delta T_i) = m\Delta T_i$$

for every i under the fully developed condition, and m is the number of cells. The axial heat transfer per unit depth Q_a of the channel during one cycle is given by $2(B-\delta B)\delta L\rho C_p\delta T$, and thus the effective thermal conductivity λ_{eff} is defined as

$$Q_a \equiv \lambda_{\text{eff}}(\Delta T/L)2B2\delta t = 2(B-\delta B)\delta L\rho C_p\delta T. \tag{25}$$

Substituting equation (24) into equation (25), we obtain the effective thermal diffusivity κ_{eff}

$$\kappa_{\text{eff}} \equiv \lambda_{\text{eff}}/\rho C_p = f\delta L^2\zeta(1-\zeta)\frac{1-\exp(-1/2f\tau)}{1+\exp(-1/2f\tau)}. \tag{26}$$

When the effective heat transfer coefficient α_{eff} is given by experiments and/or simulations, we can estimate the effective thermal diffusivity, the axial heat flux and the temperature response.

4.4. *Effective heat transfer coefficient*

The effective heat transfer coefficient α_{eff} is given by using equations (15) and (26)

$$\alpha_{\text{eff}} = 2fB\rho C(1-\zeta)\zeta\ln\left[\frac{f\delta L^2\zeta(1-\zeta)+\kappa_{\text{eff}}}{f\delta L^2\zeta(1-\zeta)-\kappa_{\text{eff}}}\right] \tag{27}$$

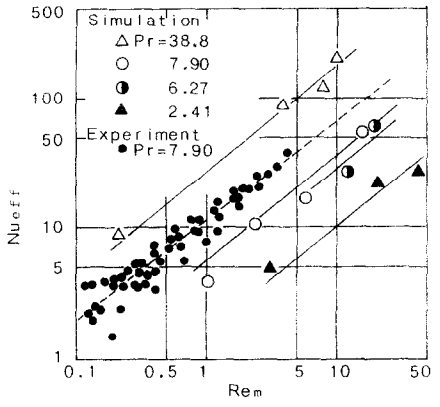

FIG. 8. Effective heat transfer coefficient.

where the effective thermal diffusivity κ_{eff} should be less than the value $f\delta L^2\zeta(1-\zeta)$.

Substituting the effective thermal diffusivity κ_{eff} obtained in the numerical simulation into equation (27), the effective heat transfer coefficient α_{eff} is obtained. Figure 8 shows the relationship between the Nusselt number Nu_{eff} and the modified Reynolds number Re_m defined by

$$Nu_{eff} = 2\alpha_{eff}B(1-\zeta)/\lambda \tag{28}$$

$$Re_m = [4f\Delta LB/\nu][2B(1-\zeta)^2/\Delta L]^2 \tag{29}$$

where the chosen representative length is $2B(1-\zeta)$ and the representative velocity is $2f\delta L$. The term in the second square bracket of equation (29) represents the entrance effect in each cell which is deduced based on the assumption that the heat transfer in such a flow field is similar to that in a developing region of forced convective flow.

The value of Nu_{eff} obtained in the numerical simulation increases exponentially with increasing Re_m. Moreover, Nu_{eff} increases with increasing the Prandtl number Pr, i.e. the Nusselt number is approximately proportional to the Prandtl number, $Nu_{eff} \propto Pr$, which is a remarkable feature in the present problem. In a forced convective flow, the Nusselt number is proportional to, for example, $Pr^{1/3}$, which is mainly due to the fact that the thickness of the thermal boundary layer is a function of the Prandtl number. On the other hand, both the boundary layer thicknesses approximately coincide with each other in the present system. Thus, the lateral heat transfer in the system with sinusoidal fluid motion approximately corresponds to the situation of $Pr \simeq 1$ in a forced convective flow. Almost all data obtained in the numerical simulation can be correlated by the solid lines which are expressed by

$$Nu_{eff}/Pr = 0.678Re_m^{0.818}. \tag{30}$$

The application of this equation is limited in the range of the simulation results, i.e. $Pr = 2$–40 and $Re_m = 0.1$–50.

5. EXPERIMENT IN A VERTICAL PIPE

5.1. *Experiment*

The experimental setup is almost the same as shown in Fig. 3. The test section in this case was the Plexiglas pipe of 1 m in length and the pipe dimensions were 3.4 mm i.d., 12.9 mm o.d. and 4.7 mm i.d., 10 mm o.d. The test section was thermally insulated. The heating pipe in the upper plenum was removed in the present experiment to enable the circulation of constant-temperature water from the thermostat through the upper plenum. The working fluid was water. It was rather difficult to measure the axial heat flux in the present system. Thus the temperature histories under the transient conditions were obtained at several positions along the pipe, and the effective thermal diffusivities were estimated to represent the heat transfer performance.

The experimental procedure was as follows: firstly, constant-temperature water of T_L from the thermostat was circulated throughout the whole test pipe, while the hot water of T_H from another thermostat was isolated from the upper plenum. When the temperature throughout the test section reached T_L, the water circulation through the test pipe was stopped and lower temperature water was circulated only through the cooling pipe in the lower plenum. Then the hot water of T_H was circulated through the upper plenum. This situation corresponds to that of the numerical simulation discussed in Section 4. After a few minutes the temperature in the upper plenum reached an approximately constant value, and the fluid oscillation was imposed. Then, the temperatures at several positions were recorded.

The experiment was carried out under the conditions of the temperatures $T_H \simeq 28.0$°C and $T_L \simeq 10.0$°C, the superficial amplitude $\Delta L = 0.081$–0.325 m and the frequency $f = 0.32$–3.4 Hz. The room temperature was about 16°C. The heat transfer coefficient at the inner wall of the pipe is expected to be rather high, and the heat loss or the heat input from the pipe wall is dominated by the heat conduction and the heat capacity of the pipe wall. The thermal diffusivity of the Plexiglas is of the order of 10^{-5} m^2 s^{-1}, while the effective thermal diffusivity obtained in the experiment is 10^{-3}–10^{-2} m^2 s^{-1} as shown in Fig. 10. The heat flux to or from the pipe wall is expected to be relatively small compared with the axial heat flux. Thus the data processing was carried out under the assumption of the adiabatic wall. This will cause an error in estimating the effective thermal diffusivity for relatively small values of f and ΔL. Further investigation will be needed on this matter. The temperature change was relatively large in the time and space in the present experiment, and therefore the mean temperature 19°C of T_H and T_L was chosen as the representative temperature for the estimation of the thermo-physical properties of water. The difference between this representative temperature and T_H or T_L results in, for example, the difference in the

thickness of the depth of penetration of about 10%. The reproducibility of the experiment was relatively good and the scatters of the settling temperature T_s and the delay time τ_d were within ± 0.3 K and $\pm 5\%$, respectively.

The temperature history in every position along the test section showed similar behavior to that shown in Fig. 5, i.e. the fluid temperature in each position increased with oscillation, and the amplitude of the temperature oscillation increased at lower position and decreased at higher position. Based on the same idea as in the numerical simulation, we obtained the delay time τ_d. The delay time τ_d in the case of $D = 4.7$ mm is plotted against the frequency in Fig. 9. The delay time τ_d decreases with the increase in the frequency f and the superficial amplitude ΔL. This behavior was also observed in the case of $D = 3.4$ mm.

The delay time is affected, of course, by the heat conduction of water as well as of the Plexiglas pipe. Since the thermal diffusivities of water and Plexiglas are 1.41×10^{-7} and 1.21×10^{-5} m^2 s^{-1}, respectively, the delay times τ_d of heat conduction are 6.74×10^5 and 7850 s, respectively. These values are quite large relative to those in the present experiment. Thus, the present data can be considered to be dominated by the heat transfer enhanced due to the fluid oscillation.

The effective thermal diffusivity κ_{eff} was calculated by using equations (8) and (9) based on the same concept as in the numerical simulation. The effective thermal diffusivity κ_{eff} enhanced by oscillation is plotted against the oscillation frequency f in Fig. 10. The parameter is the superficial amplitude ΔL. The effective thermal diffusivity κ_{eff} is in the order of 10^{-3}–10^{-2}, which corresponds to 10–100 times higher than that of copper. The effective thermal diffusivity κ_{eff} increases with the increase in the frequency f as well as in the superficial amplitude ΔL.

By using this effective thermal diffusivity, the effective heat transfer coefficient is estimated in a similar manner to that described in Section 4. In this experiment, a pipe was used as the test channel, and therefore equations (15) and (26) for the two-dimensional system cannot be applicable to this pipe flow. Thus, the effective thermal diffusivity is formulated using a pipe flow model.

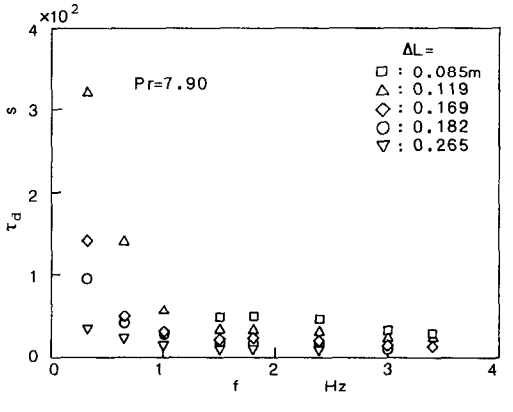

FIG. 9. Delay time (experiment in pipe, $D = 4.7$ mm, $L = 1.0$ m).

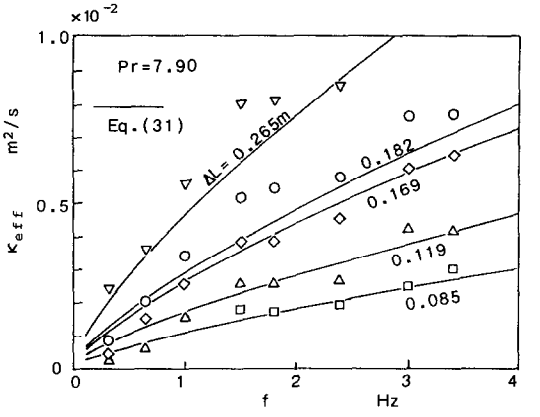

FIG. 10. Effective thermal diffusivity (experiment in pipe, $D = 4.7$ mm, $L = 1.0$ m).

5.2. *Lumped-parameter model for pipe flow and lateral heat transfer*

The lumped-parameter model for the pipe flow is quite similar to that for the two-dimensional model, so only the important equations are described here.

The effective thermal diffusivity for the pipe flow is expressed by

$$\kappa_{eff} = 2f\delta L^2(1-\xi)^2 \frac{\xi}{1+\xi} \frac{1-\exp(-1/2f\tau)}{1+\exp(-1/2f\tau)} \tag{31}$$

where $\xi = \delta r/r$, r represents the radius of pipe, δr the depth of penetration which is given by the same equation as equation (5), $\delta r = \sqrt{(\nu/\pi f)}$, $\delta L = \Delta L/(1-\xi)^2$, and the characteristic time constant τ is given by

$$\tau = \frac{\xi(1-\xi)\rho C_p r}{(1+\xi)\alpha_{eff}}. \tag{32}$$

Rearranging equations (31) and (32), we have the equation for α_{eff} just as in the two-dimensional model.

The Nusselt number Nu_{eff} obtained by using the above equations, and the experimental results, are plotted against the modified Reynolds number Re_m in Fig. 8. The Nusselt number and the modified Reynolds number for the pipe flow are defined by

$$Nu_{eff} = 2r(1-\xi)\alpha_{eff}/\lambda \tag{33}$$

$$Re_m = \frac{4f\Delta L r}{(1-\xi)\nu}\left[\frac{2r(1-\xi)^3}{\Delta L}\right]^2. \tag{34}$$

Most of the data are accurately represented by the broken line independently of the pipe diameter. The inclination of the broken line, i.e. the exponent of Re_m of the pipe flow, is slightly smaller than that of the

two-dimensional model. The correlation line for the pipe flow is expressed by

$$Nu_{\text{eff}} = 11.54 Re_{\text{m}}^{0.768}. \quad (35)$$

Similar to forced convective heat transfer, it is postulated that the dependence on the Prandtl number in the pipe flow is the same as that in the two-dimensional flow. Then the correlation equation (35) is rewritten as

$$Nu_{\text{eff}}/Pr = 1.46 Re_{\text{m}}^{0.768}. \quad (36)$$

It is expected that the application of this equation is limited in the range of $Pr = 2$–40 and $Re_{\text{m}} = 0.1$–50.

By applying this relationship, we can estimate the effective thermal diffusivity when designing such heat transfer equipment. One such example estimated by using equations (31), (32) and (36) is shown by solid lines in Fig. 10. The axial heat flux as well as the transient temperature response can also be estimated by using the present lumped-parameter model and equation (36).

6. CONCLUSION

Heat transfer characteristics in a channel with sinusoidal fluid motion were investigated. The numerical simulation suggested that the thermal boundary layer thickness approximately coincided with that of the velocity boundary layer. This situation approximately corresponded to that of the Prandtl number to be unity in a forced convective heat transfer. Based on the heat transfer mechanism postulated in the numerical simulation, the simplified lumped-parameter model was developed and the effective thermal diffusivity was formulated. By using the experimental results and the results in the numerical simulation, the effective heat transfer coefficient between the bulk and the region of the depth of penetration was correlated. The present results will contribute to the design and control of heat transfer equipment which is enhanced by sinusoidal fluid oscillation.

Acknowledgements—The authors wish to express their sincere thanks to Professors T. Sakaguchi, K. Akagawa and H. Hamaguchi, and Mr A. Ichii for their helpful suggestions. Thanks are also extended to Mr S. Ono for his assistance in carrying out experiments and to Dr A. Tomiyama for his assistance with the numerical simulations.

REFERENCES

1. U. H. Kurzweg and Ling de Zhao, Heat transfer by high frequency oscillations: a new hydrodynamic technique for achieving large effective thermal conductivities, *Physics Fluids* **27**, 2624–2627 (1984).
2. U. H. Kurzweg, Enhanced heat conduction in fluids subjected to sinusoidal oscillations, *Trans. ASME, J. Heat Transfer* **107**, 459–462 (1985).
3. U. H. Kurzweg, Temporal and spatial distribution of heat flux in oscillating flow subjected to an axial temperature gradient, *Int. J. Heat Mass Transfer* **29**, 1969–1977 (1986).
4. J. G. Zhang and U. H. Kurzweg, Numerical simulation of time-dependent heat transfer in oscillating pipe flow, *Proc. AIAA/ASME 5th Joint Thermodynamics and Heat Transfer Conf.*, Paper No. AIAA 90-1774. AIAA (1990).
5. H. Schlichting, *Boundary-layer Theory*, p. 85. McGraw-Hill, New York (1968).
6. A. Tomiyama, Y. Ichikawa, K. Morioka and T. Sakaguchi, A numerical method for solving natural-convection dominating flows, *Trans. JSME* **57**(538), 2054–2059 (1991).
7. Y. Kodaira, *Mathematics for Physics* (*Buturi-Sugaku*), Vol. 2, p. 289. Bunken-sha, Tokyo (1971).

MODELISATION A PARAMETRE LOCALISE DU TRANSFERT DE CHALEUR ACCRU PAR MOUVEMENT SINUSOIDAL DU FLUIDE

Résumé—On augmente fortement le transfert thermique axial en imposant un mouvement sinusoïdal à un fluide dans un tube. Ceci provient de la diffusion latérale de la chaleur de la capacité d'accumulation de la chaleur dans un région de profondeur de pénétration formée près de la paroi et du mouvement de convection forcée par les oscillations. La simulation numérique et la visualisation du champ thermique donne une explication phénoménologique du mécanisme fondamental du transfert de chaleur. La diffusivité thermique effective dans la direction axial est formulée, basée sur le modèle de paramètre localisé et la relation constitutive du transfert thermique latéral est dérivée de la simulation et de l'expérience.

MODELLIERUNG DES VERBESSERTEN WÄRMEÜBERGANGS BEI SINUSFÖRMIGER FLUIDBEWEGUNG MIT HILFE KONZENTRIERTER PARAMETER

Zusammenfassung—Der axiale Wärmetransport in einem Rohr wird durch Überlagerung einer sinusförmigen Fluidbewegung stark verbessert. Dies ist hauptsächlich auf seitliche Wärmeleitung, die Wärmespeicherung in einem wandnahen Gebiet und konvektive Fluidbewegung infolge der Oszillation zurückzuführen. Numerische Berechnungen und die Sichtbarmachung des Wärmestroms ermöglichen eine phänomenologische Erklärung der grundlegenden Wärmetransportmechanismen. Die effektive Temperaturleitfähigkeit in axialer Richtung wird auf der Grundlage eines Wärmetransportmodells mit konzentrierten Parametern beschrieben. Die Beziehung für den seitlichen Wärmetransport wird aus Simulation und Experiment ermittelt.

МОДЕЛИРОВАНИЕ ТЕПЛОПЕРЕНОСА, ИНТЕНСИФИЦИРОВАННОГО СИНУСОИДАЛЬНЫМ ДВИЖЕНИЕМ ЖИДКОСТИ, С ИСПОЛЬЗОВАНИЕМ СОСРЕДОТОЧЕННЫХ ПАРАМЕТРОВ

Аннотация—Предложен способ значительной интенсификации аксиального теплопереноса посредством наложения синусоидального движения на жидкость в трубе. Интенсификация происходила преимущественно за счет поперечной диффузии тепла, его способности аккумулироваться вблизи стенки, а также за счет конвективного течения, вызванного осцилляцией. Численное моделирование и визуализация теплового потока дают феноменологическое объяснение основного механизма теплопереноса. На основе модели теплопереноса с использованием сосредоточенных параметров формулируется эффективная температуропроводность в осевом направлении и выводятся соотношения для поперечного теплопереноса.